Tailored martensitic transformation and enhanced magnetocaloric effect in all-*d*-metal $Ni_{35}Co_{15}Mn_{33}Fe_2Ti_{15}$ alloy ribbons

Yong Li(李勇), Liang Qin(覃亮), Hongguo Zhang(张红国), and Lingwei Li(李领伟)

Citation: Chin. Phys. B, 2022, 31 (**8**): 087103. DOI: 10.1088/1674-1056/ac6edf
Journal homepage: http://cpb.iphy.ac.cn; http://iopscience.iop.org/cpb

What follows is a list of articles you may be interested in

Interfacial defect engineering and photocatalysis properties of hBN/MX_2 (M = Mo, W, and X = S, Se heterostructures

Zhi-Hai Sun(孙志海), Jia-Xi Liu(刘佳溪), Ying Zhang(张颖), Zi-Yuan Li(李子源), Le-Yu Peng(彭乐宇), Peng-Ru Huang(黄鹏儒), Yong-Jin Zou(邹勇进), Fen Xu(徐芬), and Li-Xian Sun(孙立贤)

Chin. Phys. B, 2022, 31 (**6**): 067101. DOI: 10.1088/1674-1056/ac43b2

Electronic structures, magnetic properties, and martensitic transformation in all-d-metal Heusler-like alloys Cd_2MnTM(TM=Fe, Ni, Cu)

Yong Li(李勇), Peng Xu(徐鹏), Xiaoming Zhang(张小明), Guodong Liu(刘国栋), Enke Liu(刘恩克), Lingwei Li(李领伟)

Chin. Phys. B, 2020, 29 (**8**): 087101. DOI: 10.1088/1674-1056/ab9739

Large reversible magnetocaloric effect induced by metamagnetic transition in antiferromagnetic HoNiGa compound

Yi-Xu Wang(王一旭), Hu Zhang(张虎), Mei-Ling Wu(吴美玲), Kun Tao(陶坤), Ya-Wei Li(李亚伟), Tim Yan(颜天宝), Ke-Wen Long(龙克文), Teng Long(龙腾), Zheng Pang(庞铮), Yi Long(龙毅)

Chin. Phys. B, 2016, 25 (**12**): 127104. DOI: 10.1088/1674-1056/25/12/127104

Coexistence of positive and negative magnetic entropy changes in $CeMn_2(Si_{1-x}Ge_x)_2$ compounds

Zuo Wen-Liang, Hu Feng-Xia, Sun Ji-Rong, Shen Bao-Gen

Chin. Phys. B, 2015, 24 (**9**): 097104. DOI: 10.1088/1674-1056/24/9/097104

The effect of Fe on the martensitic transformation of TaRu high-temperature shape memory alloys:A first-principles study

Tan Chang-Long(谭昌龙), Tian Xiao-Hua (田晓华), and Cai Wei(蔡伟)

Chin. Phys. B, 2012, 21 (**5**): 057105. DOI: 10.1088/1674-1056/21/5/057105

Tailored martensitic transformation and enhanced magnetocaloric effect in all-*d*-metal $Ni_{35}Co_{15}Mn_{33}Fe_2Ti_{15}$ alloy ribbons

Yong Li(李勇)[1,†], Liang Qin(覃亮)[1], Hongguo Zhang(张红国)[2], and Lingwei Li(李领伟)[1]

[1] *Key Laboratory of Novel Materials for Sensor of Zhejiang Province, College of Materials & Environmental Engineering, Hangzhou Dianzi University, Hangzhou* 310018, *China*

[2] *Faculty of Materials and Manufacturing, Key Laboratory of Advanced Functional Materials, Ministry of Education of China, Beijing University of Technology, Beijing* 100124, *China*

(Received 4 March 2022; revised manuscript received 7 May 2022; accepted manuscript online 12 May 2022)

The crystal structure, martensitic transformation and magnetocaloric effect have been studied in all-*d*-metal $Ni_{35}Co_{15}Mn_{33}Fe_2Ti_{15}$ alloy ribbons with different wheel speeds (15 m/s (S15), 30 m/s (S30), and 45 m/s (S45)). All three ribbons crystalize in B2-ordered structure at room temperature with crystal constants of 5.893(2) Å, 5.898(4) Å, and 5.898(6) Å, respectively. With the increase of wheel speed, the martensitic transformation temperature decreases from 230 K to 210 K, the Curie temperature increases slightly from 371 K to 378 K. At the same time, magnetic entropy change (ΔS_m) is also enhanced, as well as refrigeration capacity (*RC*). The maximum ΔS_m of 15.6(39.7) J/kg·K and *RC* of 85.5 (212.7) J/kg under $\Delta H = 20$ (50) kOe (1 Oe = 79.5775 A·m^{-1}) appear in S45. The results indicate that the ribbons could be the candidate for solid-state magnetic refrigeration materials.

Keywords: martensitic transformation, magnetocaloric effect, wheel speeds, all-*d*-metal Heusler ribbons

PACS: 71.15.Mb, 31.15.A–, 71.20.–b, 75.20.En **DOI:** 10.1088/1674-1056/ac6edf

1. Introduction

Magnetic materials with outstanding magnetoresponsive performances have been attracted researchers' interest in recent years.[1–5] Among them, compared to conventional refrigeration technologies based on vapor compression which have caused the environmental pollution and greenhouse effect, the solid-state magnetic refrigeration (MR) technologies,[6–18] based on the magnetocaloric effect (MCE), have been shown as high efficiency alternative and environmentally friendly method that we seek in sustainable society. Until now, several materials based on first-order magnetostructural transitions (FOMSTs) with large MCE have been reported, including rare earth (*RE*)-based compounds,[12,14,19] Hexagonal MM'X alloys,[20,21] and Heusler alloys,[22,23] *etc.* Searching and designing novel magnetic materials with outstanding magnetocaloric performance is one of the topic issues at present stage.

In 2015, Wei *et al.*[24] reported a new alloy system with FOMSTs named all-*d*-metal Heusler alloys, substituting *p*–*d* orbital hybridization between main-group element and transition group element (Al, Ga, In, *etc.*) by *d*–*d* orbital hybridization between transition group elements (Ni with high valence-electrons and Ti with low valence-electrons), which has accelerated the exploration of new multifunctional materials. The *d*–*d* orbital hybridization can also stabilize parent phase structure and introduced Co atoms make the establishment of ferromagnetism.[25] Subsequently, Bez *et al.*[26] reported that solidified ribbons exhibit magnetic entropy change (ΔS_m) as high as 27 J/kg·K with magnetic field change of 20 kOe in $Ni_{37.5}Co_{12.5}Mn_{35}Ti_{15}$. Using digital image correlation and infrared thermography technologies, Wei *et al.*[27] observed irreversible (reversible) ΔT_{ad} of 10.7 K (9.0 K) at a strain level of 3.9% (4.6%) for $Ni_{50}Mn_{32}Ti_{18}$ and $Ni_{35}Co_{15}Mn_{35}Ti_{15}$, respectively. At the same time, the prediction of crystal and electronic behaviors, phase stability, magnetic state, and possible martensitic transformation (MT) have also been calculated by the first principle calculations based on density functional theory (DFT) to explore the more all-*d*-metal Heusler alloys.[28,29] Most of them are focused on the modification of chemical composition, thermal treatment, and pressure in the all-*d*-metal alloys. For ribbon samples, little attention has been focused on the effect of linear wheel speed on MT and MCE.

Improving phase compatibility and minimizing thermal hysteresis between the martensite and the austenite through hydrostatic pressure and/or chemical substitutions (such as Fe element) have been reported.[5,26,30] In this work, the effect of wheel speeds (15 m/s, 30 m/s, and 45 m/s) on the crystal structure, MT and mangetocaloric properties in $Ni_{35}Co_{15}Mn_{33}Fe_2Ti_{15}$ ribbons are systematically investigated. With the increase of wheel speed, the grain size becomes smaller resulting in the decrease of martensitic transformation temperature (T_t) from 230 K to 210 K, *i.e.*, the austenite is stabilized. Meanwhile, Curie temperature of martensite (T_C^A) slightly increases from 371 K to 378 K. It is worth noting that the enhancement of ΔS_m of 15.6 (39.7) J/kg·K and refrigeration capacity (*RC*) of 85.5 (212.7) J/kg with magnetic field change of 20 (50) kOe can be obviously obtained for S45, the values are comparable or even larger than some reported mag-

†Corresponding author. E-mail: yongli@hdu.edu.cn

netocaloric materials.

2. Experimental details

With high purity metals ($\geq$ 99.9%), the polycrystalline $Ni_{35}Co_{15}Mn_{33}Fe_2Ti_{15}$ alloy ingot was fabricated by arc-melting method under the argon atmosphere. The alloy ingot was turned and re-melted for 4-times to ensure homogeneity and then cut into three pieces. The Mn losses were compensated for by adding the excess of Mn elements. The three ribbons, ejecting (ejection pressure of $\sim$ 0.1 MPa) the ingots onto a rotating copper wheel with a surface speed of 15 m/s (S15), 30 m/s (S30), and 45 m/s (S45), were prepared by using melt-spinning techniques as studied samples. The scanning electron microscope (SEM, Sigma 300, Zeiss) with x-ray energy-dispersive spectroscopy (EDS) was carried out to investigate the microstructure and composition of melt-spun ribbons. The crystal structures were investigated by room temperature (RT) x-ray diffiraction (XRD, SmartLab-9 kW, Rigaku) with Cu-K_α radiation. The differential scanning calorimeter (DSC, Discovery DSC 25, TA) was used to measure thermal property. The microstructure was measured by using scanning electron microscope (SEM, Sigma-300, Zeiss). The magnetization data (thermomagnetic (M–T) curves and isothermal magnetization (M–H) curves) were obtained by magnetic property measurement system (MPMS3, Quantum Design).

3. Results and discussion

The microstructure of free surface using SEM at room temperature (RT) is depicted in Figs. 1(a)–1(c) for $Ni_{35}Co_{15}Mn_{33}Fe_2Ti_{15}$ with S15, S30, and S45, respectively. The visible equiaxed-grain-like austenite without the appearance of plat-like martensite can be clearly seen. The average grain size obviously declines from 3.5 μm (S15) to 2.8 μm (S30) and further to 1.0 μm (S45) with increasing wheel speed, *i.e.*, lower grain size with higher cooling rate. RT XRD patterns of $Ni_{35}Co_{15}Mn_{33}Fe_2Ti_{15}$ with different wheel speeds are shown in Fig. 1(d). The similar phenomenon can be seen for all ribbons. Due to absence of the superlattice diffraction peaks of $L2_1$ structure, all three ribbons crystalize in B2-ordered structure which is similar to other reported all-*d*-metal Heusler alloys,[24,31] meaning that the ribbons prefer to form B2 rather than $L2_1$ structure during melt spun process. It also indicates that the martensitic transformation temperature (T_t) is below RT, which is conformed to SEM analysis. The miller indexes of (220), (400), (422) are signed in the corresponding peaks. The characteristic peaks move slightly towards to small angle with increasing wheel speed, the crystal constant, 5.893(2) Å for S15, 5.898(4) Å for S30, and 5.898(6) Å for S45 (see Table 1), monotonically increases. Another is worth noting is that the more intensive intensity of the diffraction of (220) plane, showing that the $\langle 110 \rangle$ direction is closely parallel to the solidification direction, is the preferred direction during melt spun process.[32,33]

The DSC curves with different wheel speeds were measured upon heating and cooling rates of 10 K/min under nitrogen atmosphere, which are displayed in Fig. 1(e). The obviously exothermic and endothermic peaks (below RT) with thermal hysteresis appear for three ribbons, which show that the type of transition belongs to first order nature. T_t (T_t') monotonously decreases with the increase of wheel speed (Table 1), meaning that MT is sensitive to wheel speed. The T_t (T_t') of 231 (268) K for S15 decreases to 218 (246) K for S30 and further to 206 (243) K for S45.

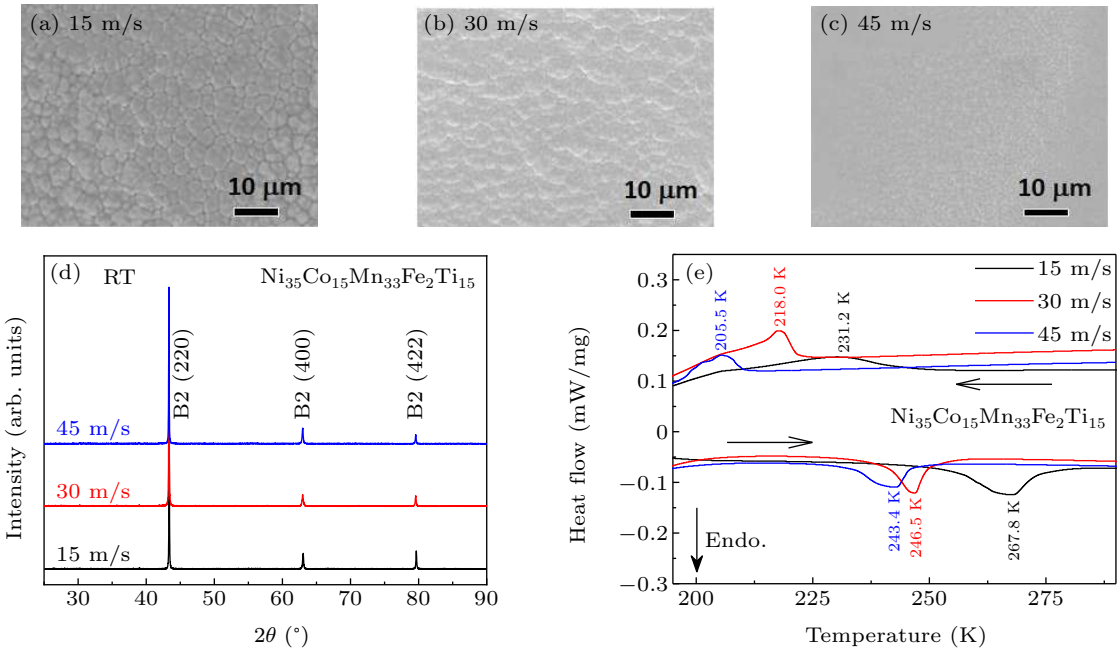

Fig. 1. (a)–(c) Microstructure of free surface using SEM, (d) room-temperature XRD patterns, and (e) DSC curves for $Ni_{35}Co_{15}Mn_{33}Fe_2Ti_{15}$ with wheel speed of 15 m/s, 30 m/s, and 45 m/s, respectively.

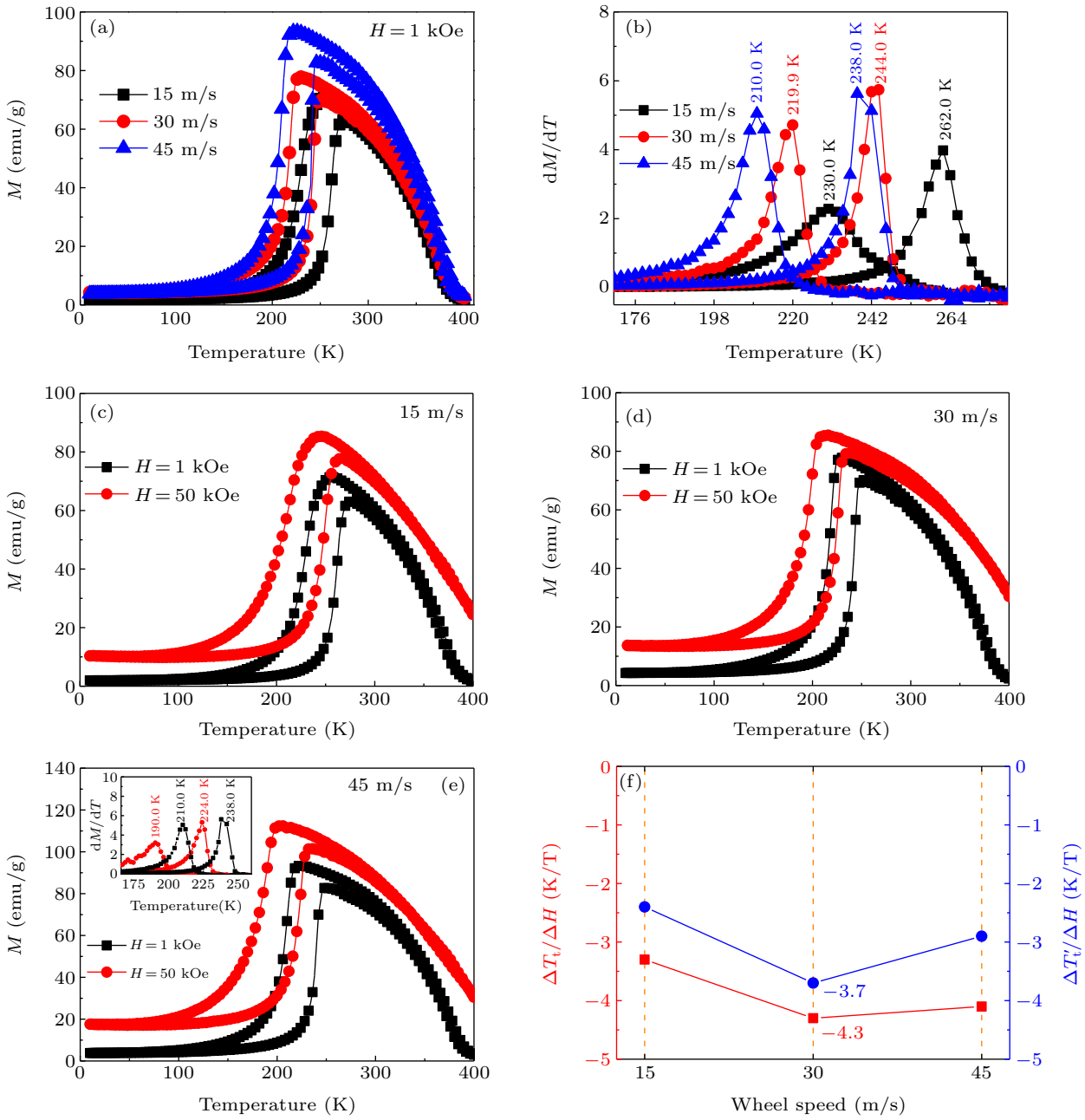

Fig. 2. (a) Thermomagnetic (M–T) curves under 1 kOe. (b) The derivative of M–T ($\mathrm{d}M/\mathrm{d}T$) curves as a function of temperature. (c)–(e) Temperature dependence of magnetization (M–T) curves under 1 kOe and 50 kOe. (f) The driving rate by magnetic field ($\Delta T_\mathrm{t}/\Delta H$, normal MT, circle; $\Delta T_\mathrm{t}'/\Delta H$, reverse MT, square) for $Ni_{35}Co_{15}Mn_{33}Fe_2Ti_{15}$ with wheel speed of 15 m/s, 30 m/s, and 45 m/s, respectively.

The thermomagnetic (M–T) curves were measured at 5 K/min in a magnetic field of 1 kOe between 10 K and 400 K, as depicted in Fig. 2(a). The three ribbons, upon cooling process, firstly undergo the Curie temperature in austenite (T_C^A) from paramagnetic state to FM state. Subsequently, a magnetostructural transitions happen accompanied by a sudden drop of magnetization from FM austenite to weak-magnetic (WM) martensite. The reverse curves upon heating are not coincided with the curves upon cooling, *i.e.*, the thermal hysteresis obviously exists, indicating the characteristic of first order transition.[34] Herein, to gain the T_t (T_t') and T_C^A values, the derivative of M–T curves ($\mathrm{d}M/\mathrm{d}T$) was performed and the pattern is shown in Fig. 2(b). The results show that the T_t (T_C^A) is sensitive (insensitive) to the wheel speed. With the increase of wheel speed, the T_t (T_t') monotonously declines from 230 (262) K for S15 to 210 (238) K for S45, which are basically in good agreement with the values from DSC. The T_C^A (371 K for S15, 374 K for S30, and 378 K for S45) slightly rises simultaneously. The corresponding data are listed in Table 1. The larger wheel speed is used, the more stable the austenite keeps. More importantly, compared with S15 the thermal hysteresis declines for S30 and S45. Smaller hysteresis benefits refrigeration because a reduction in the refrigerant capacity caused by the irreversible behaviors associated with large hysteresis.[35] Furthermore, the magnetization change (ΔM) increases from 63.5 emu/g (S15) to 81.9 emu/g (S45) by

enhancement of Mn–Co–Mn interaction resulting in the more effective magnetoresponsive performance, which is benefit to the magnetic refrigeration in practice application under low magnetic field.[20]

To find out the fact what affects martensitic transformation, we analyzed possible reasons. For many FOMST alloys, the increase of grain size through heat treatment can tailor MT to high temperature, such as NiMn-based,[36–39] Cu-based[40,41] Heulser alloys, and Ni–Co–Mn–Ti.[42] Recently, Ma *et al.*[43] reported that the decline of MT for all-*d*-metal Heusler ribbons $Mn_{50}Ni_{31.5}Co_{8.5}Ti_{10}$ with increasing wheel speed results in the decrease of grain size. The atomic ratio is not obviously changed for three ribbons (EDS) and the three ribbons show very similar lattice constant with B2 structure (XRD), which give rise to the unchanged valence electron concentration (e/a) and ordering. The e/a value and ordering should not be taken into account in the presented case. Therefore, the grain size in three ribbons should play important role. The reason is similar to Mn–Fe–Ni–Ge–Si[44] and $Mn_{50}Ni_{31.5}Co_{8.5}Ti_{10}$,[43] during the MT the strain energy stored in the material is produced by shearing and by volume change totally, the more produced defects with increasing wheel speed result in the smaller grain size, then the more large driving force was needed to complete MT process. Therefore, the MT shifts to low temperature with increasing wheel speed, *i.e.* increase of wheel speed can stabilize parent phase.[39]

Table 1. The values of T_t (T_t'), T_{hys}, ΔT_t ($\Delta T_t'$), and $\Delta T_t/\Delta H$ ($\Delta T_t'/\Delta H$) using DSC under zero magnetic field and MPMS under the fields of 1 kOe and 50 kOe for $Ni_{35}Co_{15}Mn_{33}Fe_2Ti_{15}$ with wheel speed of 15m/s, 30 m/s and 45 m/s, respectively.

Wheel speed	XRD	DSC			MPMS										
					$H = 1$ kOe				$H = 50$ kOe						
	a (Å)	T_t (K)	T_t' (K)	T_{hys} (K)	T_t (K)	T_t' (K)	T_{hys} (K)	T_C^A (K)	T_t (K)	T_t' (K)	T_{hys} (K)	ΔT_t (K)	$\Delta T_t'$ (K)	$\Delta T_t/\Delta H$ (K/T)	$\Delta T_t'/\Delta H$ (K/T)
15 m/s (S15)	5.893(2)	231	267	36	230	262	32	371	214	250	36	−16	−12	−3.3	−2.4
30 m/s (S30)	5.898(4)	218	246	28	220	244	24	374	198	226	28	−21	−18	−4.3	−3.7
45 m/s (S45)	5.898(6)	205	243	36	210	238	28	378	190	224	34	−20	−14	−4.1	−2.9

*a: lattice constant at room temperature; T_t, T_t': normal/reverse MT temperature; T_{hys}: difference between T_t' and T_t; T_C^A: Curie temperature in austenite; ΔT_t, $\Delta T_t'$: change of T_t and T_t' with increasing magnetic field from 1 kOe to 50 kOe; $\Delta T_t/\Delta H$, $\Delta T_t'/\Delta H$: Driving rate by magnetic field for normal/reverse MT.

Figures 2(c)–2(e) display the thermomagnetic (M–T) curves recorded under magnetic fields of 1 kOe and 50 kOe between 10 K and 400 K for $Mn_{50}Ni_{31.5}Co_{8.5}Ti_{10}$ with S15, S30, and S45, respectively. It is worth noting that the ferromagnetism of austenite is stronger than that of martensite, the T_t (T_t') calculated from the inset of Fig. 2(e) obviously declines with increase of external magnetic field owing to the transformation from FM to WM state. The behaviors result from the magnetic field stabilizing the phase with a higher magnetization by introducing Zeeman energy, *i.e.*, magnetic field stabilizes parent phase in the system. The results are similar to many conventional Heusler shape memory alloys, just like Ni–Mn–In,[45] Ni–Co–Mn–In,[46] Co–V–Ga,[47] and Ni–Mn–Sn.[48] The maximum changes of T_t (T_t') induced by magnetic field ($\Delta T_t/\Delta H$, $\Delta T_t'/\Delta H$) can reach −4.3 (−3.7) K/T (Fig. 2(f), Table 1) for S30, which are compared with and even larger than other materials.[43,49,50]

For solid-state magnetic refrigeration materials, the magnetic entropy change (ΔS_m) and refrigeration capacity (RC) are important factors to determine refrigeration performance in practical applications.[6] The temperature loop method,[31,51] with the temperature step (ΔT) of 3 K, was used in vicinity of MST to eliminate the residual effect generated in previous measurement and avoid overestimating the ΔS_m. Figure 3(a) displays the isothermal magnetization (M–H) curves for S15 measured around reverse MT. Below T_t, the quasi-linear increased magnetization under a magnetic field up to 50 kOe indicates the weak-magnetic behavior. The magnetic hysteresis is low due to the absence of change of magnetization induced by variation between austenite and martensite. Above T_t, characteristic FM behaviors with low saturation-field of austenite can be observed, showing that the samples are easy to be magnetized and saturated with increasing magnetic field. In the vicinity of T_t, obviously magnetic-field-induced reverse MT, with critical field (H_{cr}) of 42 kOe, can be seen, the feature of metamagnetic transformation with obvious magnetic hysteresis appears.

Based on the isothermal magnetization (M–H) curves, the values of ΔS_m are calculated using the formula of intergrated Maxwell relation:[51] $\Delta S_m = S_m(T,H) - S_m(T,0) = \int_0^H (\partial M/\partial T)_H \, dH$. The ΔS_m as a function of temperature is depicted in Figs. 3(b)–3(d) for $Ni_{35}Co_{15}Mn_{33}Fe_2Ti_{15}$ with S15, S30, and S45 in the field change of 50 kOe, respectively. The positive ΔS_m originated from the ΔM between austenite and martensite when MT happens. The maximum value of ΔS_m appears at about 225 K for S30 (S45) and 255 K for S15, which is consistent with M–T curves. For S15, the maximum value of ΔS_m reaches 7.2 (18.6) J/kg·K with $\Delta H =$ (20) 50 kOe. For S30, the maximum ΔS_m increases slightly to 7.3 (19.8) J/kg·K with $\Delta H =$ (20) 50 kOe. As increase wheel speed further to 45 m/s, visible enhancement of ΔS_m can be achieved as optimal value among three wheel speeds, The value reaches 15.6 (39.7) J/kg·K with $\Delta H =$ (20) 50 kOe, respectively.

Table 2. The values of ΔS_m and *RC* under the field change of 50 kOe for $Ni_{35}Co_{15}Mn_{33}Fe_2Ti_{15}$ and reported magnetocaloric materials, respectively.

Compounds		ΔS_m (J/kg·K) (0 kOe–50 kOe)	*RC* (J/kg) (0 kOe–50 kOe)	References
$Ni_{35}Co_{15}Mn_{33}Fe_2Ti_{15}$	15 m/s (S15)	18.6	191.9	this work
	30 m/s (S30)	19	92.1	
	45 m/s (S45)	39.7	212.7	
$Ni_{35}Co_{15}Mn_{35}Ti_{15}$		18	267	[24]
$Ni_{35}Co_{11}Fe_4Mn_{35}Ti_{15}$		23	206.8	[31]
$Ni_{36.0}Co_{14.0}Mn_{35.7}Ti_{14.3}$		28	197	[42]
$Mn_{50}Ni_{31.5}Co_{8.5}Ti_{10}$		11.4	129.9	[43]
$Gd_5(Si_2Ge_2)$		14	–	[52]
$LaFe_{11.4}Si_{1.6}$		14.3	–	[53]
$Ni_{37}Co_9Fe_4Mn_{35}Ti_{15}$		5	–	[54]
$Mn_{50}Ni_{32}Co_8Ti_{10}$		16	121	[57]
$Ni_{36.5}Co_{13.5}Mn_{35}Ti_{15}$		24.9	239.7	[58]
$Ni_{37.5}Co_{12.5}Mn_{35}Ti_{15}$		27.1	–	[59]

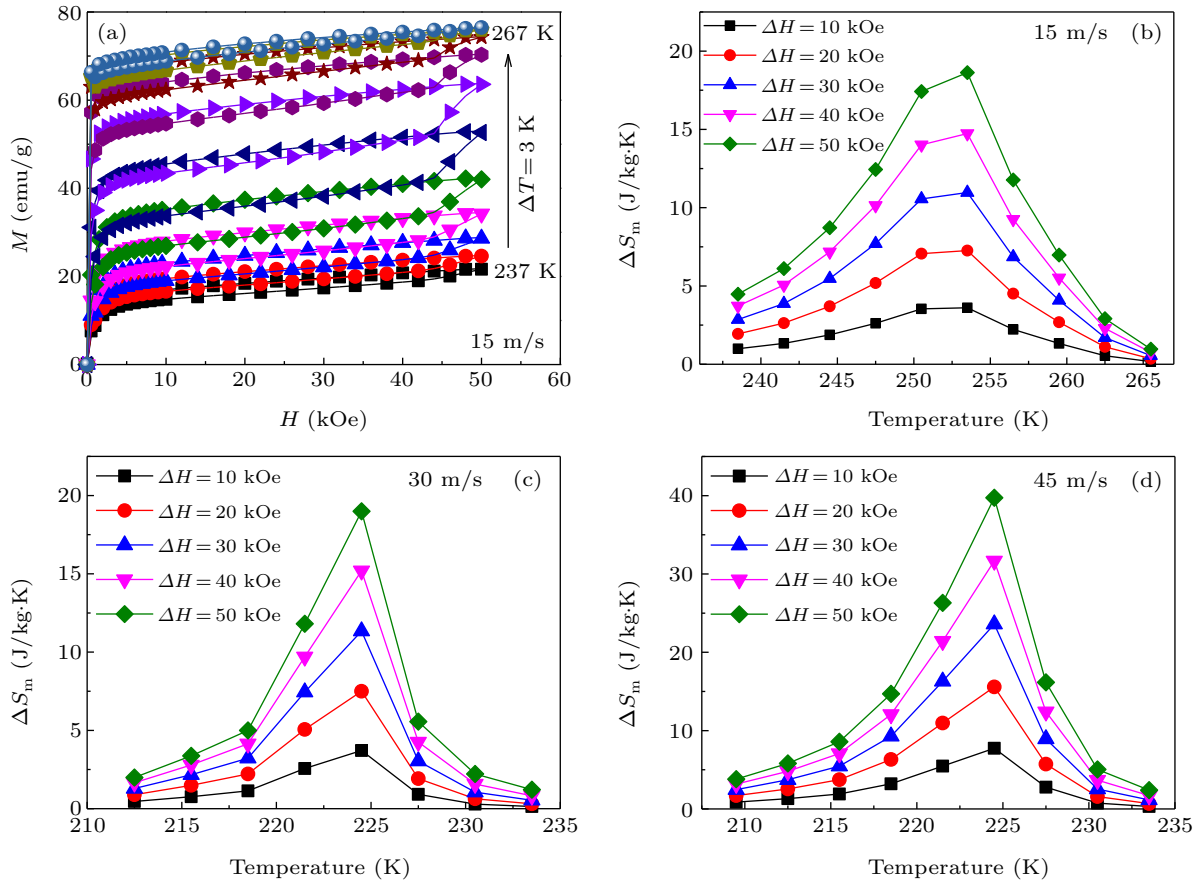

Fig. 3. (a) Isothermal magnetization (*M*–*H*) curves for $Ni_{35}Co_{15}Mn_{33}Fe_2Ti_{15}$ with wheel speed of 15 m/s. (b)–(d) Magnetic entropy changes (ΔS_m) in magnetic field change of 50 kOe for $Ni_{35}Co_{15}Mn_{33}Fe_2Ti_{15}$ with wheel speed of 15 m/s, 30 m/s, and 45 m/s, respectively.

The refrigeration capacity (*RC*), as another important factor, is used to evaluate magnetocaloric performances. According to the formula: $\Delta RC = \int_{T_1}^{T_2} |\Delta S_m| dT$, where T_1 and T_2 represent the temperatures at full width half-maximum peak (FWHM) of ΔS_m curve. For a better understanding the actual effect of wheel speed on magnetocaloric performances, the ΔS_m and *RC* as a function of magnetic field are shown in Fig. 4. The results of three parameters show the similar tendency. For ΔS_m in Fig. 4(a), we can see that the curves increase quasi-linearly and the values of ΔS_m for S45 are both obviously larger than that of S15 (S30), indicating the enhancement of magnetic-field response increasing wheel speed up to 45 m/s. The exciting enhancement of ΔS_m can be achieved for S45 as optimal value among three wheel speeds, which is more than twice compared to S15. The optimal values of ΔS_m for S45 (Table 2) are 15.6 (39.7) J/kg·K with ΔH = (20) 50 kOe and comparable with and even larger than that of reported typical magnetocaloric materials, such as 17.6 J/kg·K for $Ni_{36.3}Co_{13.7}Mn_{35}Ti_{15}$,[26] 14 J/kg·K for $Gd_5(Si_2Ge_2)$,[52] 14.3 J/kg·K for $LaFe_{11.4}Si_{1.6}$,[53] 15.9 J/kg·K for Ni_{35} $Ni_{37}Co_9Fe_4Mn_{35}Ti_{15}$,[54] and 15 J/kg·K for $Mn_{0.8}Co_{0.2}NiGe_{0.75}Si_{0.25}$[55] with ΔH = 20 kOe; and

18 J/kg·K for $Ni_{35}Co_{15}Mn_{35}Ti_{15}$,[24] and 28 J/kg·K for $Ni_{35}Cu_{2.5}Co_{12.5}Mn_{35}Ti_{15}$[42] with $\Delta H = 50$ kOe.

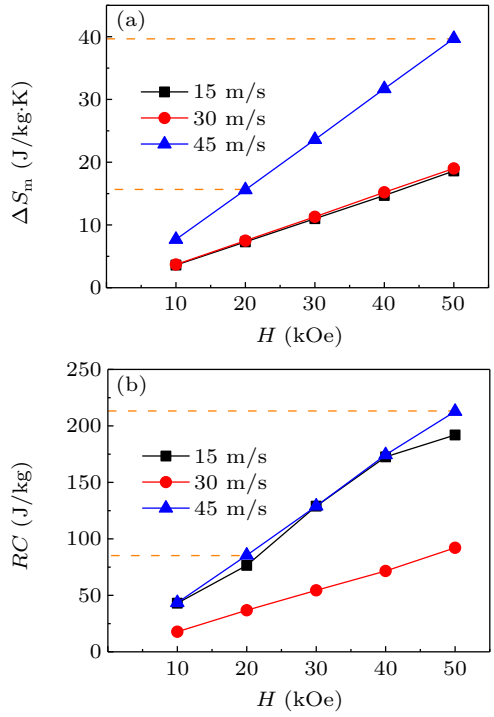

Fig. 4. Magnetic field dependence of (a) ΔS_m and (b) RC curves in the field change up to 50 kOe for $Ni_{35}Co_{15}Mn_{33}Fe_2Ti_{15}$ with wheel speed of 15 m/s, 30 m/s, and 45 m/s, respectively.

In Fig. 4(b), the RC curves also increase quasi-linearly with increasing wheel speed. The RC values reach 76.5 (191.9) J/kg and 85.5 (212.7) J/kg with $\Delta H = (20)$ 50 kOe for S15 and S45, respectively. The RC values decline to 36.8 (92.1) J/kg, nearly half of the maximum values of S15, for S30 owing to a smaller FWHM and comparative ΔS_m value calculated by two formulas above. Thus, the optimal values appear in S45 (listed in Table 2) and are comparable with and even larger than that of reported magnetocaloric materials, such as 91.5 J/kg for $Ni_{50}Mn_{32.7}Cu_{1.3}In_{16}$ with $\Delta H =$ 20 kOe[56] and 206.8 J/kg for $Ni_{35}Co_{11}Fe_4Mn_{35}Ti_{15}$,[31] 197 J/kg for $Ni_{36.0}Co_{14.0}Mn_{35.7}Ti_{14.3}$,[42] 121 J/kg for $Mn_{50}Ni_{32}Co_8Ti_{10}$,[57] 239.7 J/kg for $Ni_{36.5}Co_{13.5}Mn_{35}Ti_{15}$[58] with $\Delta H = 50$ kOe. The increase of wheel speed not only tailors MT but also enhances magnetocaloric performances (large ΔS_m and RC), which makes the all-d-metal ribbon more probable for magnetic refrigeration application.

4. Conclusion

In summary, we investigated the crystal structure, martensitic transformation, and magnetocaloric effect of all-d-metal $Ni_{35}Co_{15}Mn_{33}Fe_2Ti_{15}$ alloy ribbons with different wheel speeds (15 m/s, 30 m/s, and 45 m/s). The results indicate that three ribbons crystalize ordered B2-type cubic structure at room temperature, and crystal constant is 5.893(2) Å, 5.898(4) Å, and 5.898(6) Å, respectively. With the increase of wheel speed, the T_t declines and T_C^A slightly increases due to the decrease of grain size. More importantly, the enhanced magnetocaloric effect is also been gained. The maximum value (S45) of magnetic entropy change (ΔS_m) and refrigeration capacity (RC) are 15.6 (39.7) J/kg·K and 85.5 (212.7) J/kg in the fields of 20 (50) kOe, respectively. Therefore, $Ni_{35}Co_{15}Mn_{33}Fe_2Ti_{15}$ alloys are considerable candidate for magnetic refrigeration.

Acknowledgments

Project supported by the National Natural Science Foundation of China (Grant Nos. 52001102 and 51771003).

References

[1] Hu L, Zhu L, He H, Zhang L and Ye Z 2015 *J. Mater. Chem. C* **3** 1330
[2] Hu L, Cao L, Li L, Duan J, Liao X, Long F, Zhou J, Xiao Y, Zeng Y J and Zhou S 2021 *Mater. Horiz.* **8** 1286
[3] Tegus O, Brück E, Buschow K H J and Boer F R D 2002 *Nature* **415** 150
[4] Hou Z, Zhang Q, Zhang X, Xu G, Xia J, Ding B, Li H, Zhang S, Batra N M, Costa P, Liu E, Wu G, Ezawa M, Liu X, Zhou Y, Zhang X and Wang W 2020 *Adv. Mater.* **32** 1904815
[5] Li Y, Qin L, Huang S and Li L 2022 *Sci. China Mater.* **65** 486
[6] Li L and Yan M 2020 *J. Alloys Compd.* **823** 153810
[7] Manosa L and Planes A 2017 *Adv. Mater.* **29** 1603607
[8] Li L, Xu P, Ye S, Li Y, Liu G, Huo D and Yan M 2020 *Acta Mater.* **194** 354
[9] Zhang Y, Wu B, Guo D, Wang J and Ren Z 2021 *Chin. Phys. B* **30** 017501
[10] Wu B, Zhang Y, Guo D, Wang J and Ren Z 2021 *Ceram. Int.* **47** 6290
[11] Zhang Y, Zhu J, Li S, Wang J and Ren Z 2022 *J. Mater. Sci. Technol.* **102** 66
[12] Ma Z, Dong X, Zhang Z and Li L 2021 *J. Mater. Sci. Technol.* **92** 138
[13] Wang Y, Guo D, Wu B, Geng S and Zhang Y 2020 *J. Magn. Magn. Mater.* **498** 166179
[14] Zhang Y 2019 *J. Alloys Compd.* **787** 1173
[15] Zhang Y, Zhu J, Li S, Zhang Z, Wang J and Ren Z 2022 *Sci. China Mater.* **65** 1345
[16] Xu P, Ma Z, Wang P, Wang H and Li L 2021 *Materials Today Physics* **20** 100470
[17] Zhang Y, Tian Y, Zhang Z, Jia Y, Zhang B, Jiang M, Wang J and Ren Z 2022 *Acta Mater.* **226** 117669
[18] Hu L, Zhou J, Hou Z, Su W, Yang B, Li L and Yan M 2021 *Mater. Horiz.* **8** 3306
[19] Zou J, Shen B, Gao B, Shen J and Sun J 2009 *Adv. Mater.* **21** 693
[20] Liu E K, Wang W H, Feng L, Zhu W, Li G J, Chen J L, Zhang H W, Wu G H, Jiang C B, Xu H B and Boer F D 2012 *Nat. Commun.* **3** 873
[21] Li Y, Zeng Q, Wei Z, Liu E, Han X, Du Z, Li L, Xi X, Wang W, Wang S and Wu G 2019 *Acta Mater.* **174** 289
[22] Gottschall T, Benke D, Fries M, Taubel A, Radulov I A, Skokov K P and Gutfleisch O 2017 *Adv. Funct. Mater.* **27** 1606735
[23] Wang L, Li Z, Yang J, Yang B, Zhao X and Zuo L 2020 *Intermetallics* **125** 106888
[24] Wei Z Y, Liu E K, Chen J H, Li Y, Liu G D, Luo H Z, Xi X K, Zhang H G, Wang W H and Wu G H 2015 *Appl. Phys. Lett.* **107** 022406
[25] Wei Z Y, Liu E K, Li Y, Han X L, Du Z W, Luo H Z, Liu G D, Xi X K, Zhang H W, Wang W H and Wu G H 2016 *Appl. Phys. Lett.* **109** 071904
[26] Neves Bez H, Pathak A K, Biswas A, Zarkevich N, Balema V, Mudryk Y, Johnson D D and Pecharsky V K 2019 *Acta Mater.* **173** 225
[27] Wei Z Y, Sun W, Shen Q, Shen Y, Zhang Y F, Liu E K and Liu J 2019 *Appl. Phys. Lett.* **114** 101903
[28] Yong Li, Peng Xu, Xiaoming Zhang, Guodong Liu, Enke Liu and Li L 2020 *Chin. Phys. B* **29** 087101
[29] Taubel A, Beckmann B, Pfeuffer L, Fortunato N, Scheibel F, Ener S, Gottschall T, Skokov K P, Zhang H and Gutfleisch O 2021 *Acta Mater.* **201** 425
[30] Song Y, Chen X, Dabade V, Shield T W and James R D 2013 *Nature* **502** 85

[31] Li Y, Huang S, Wang W, Liu E and Li L 2020 *J. Appl. Phys.* **127** 233907
[32] Feng Y, Chen H, Gao L, Wang H, Bian X and Gong M 2016 *Mater. Charact.* **122** 170
[33] Li Y, Qin L, Huang S, Zhang X and Li L 2021 *J. Magn. Magn. Mater.* **529** 167891
[34] Shen Y, Wei Z, Sun W, Zhang Y, Liu E and Liu J 2020 *Acta Mater.* **188** 677
[35] Shamberger P J and Ohuchi F S 2009 *Phys. Rev. B* **79** 144407
[36] Chen L, Hu F X, Wang J, Bao L F, Zheng X Q, Pan L Q, Yin J H, Sun J R and Shen B G 2013 *J. Alloys Compd.* **549** 170
[37] Bruno N M, Huang Y J, Dennis C L, Li J G, Shull R D, Ross J H Jr, Chumlyakov Y I and Karaman I 2016 *J. Appl. Phys.* **120** 075101
[38] Zheng H, Wu D, Xue S, Frenzel J, Eggeler G and Zhai Q 2011 *Acta Mater.* **59** 5692
[39] Quintana-Nedelcos A, Llamazares J L S, Ríos-Jara D, Lara-Rodríguez A G and García-Fernández T 2013 *Phys. Stat. Sol. (a)* **210** 2159
[40] Roca P M L, Isola L M, Sobrero C E, Vermaut Ph and Malarría J 2015 *Mater. Today: Proc.* **2** S743
[41] Roca P L, Isola L, Vermaut Ph and Malarría J 2017 *Scripta Mater.* **135** 5
[42] Liu K, Han X, Yu K, Ma C, Zhang Z, Song Y, Ma S, Zeng H, Chen C, Luo X, Rehman S U and Zhong Z 2019 *Intermetallics* **110** 106472
[43] Ma C, Liu K, Han X, Yang S, Ye N and Tang J 2020 *J. Magn. Magn. Mater.* **493** 165733
[44] Liu K, Ma S C, Ma C C, Yang S, Ge Q, Han X Q, Yu K, Song Y, Zhang Z S, Chen C C, Liu E K and Zhong Z C 2018 *J. Alloys Compd.* **746** 503
[45] Li Z, Li Z, Li D, Yang J, Yang B, Hu Y, Wang D, Zhang Y, Esling C, Zhao X and Zuo L 2020 *Acta Mater.* **192** 52
[46] Kainuma R, Imano Y, Ito W, Sutou Y, Morito H, Okamoto S, Kitakami O, Oikawa K, Fujita A, Kanomata T and Ishida K 2006 *Nature* **439** 957
[47] Liu K, Ma S, Zhang Y, Zeng H, Yu G, Luo X, Chen C, Rehman S U, Hu Y and Zhong Z 2020 *J. Mater. Sci. Technol.* **58** 145
[48] Zhang G, Li Z, Yang J, Yang B, Wang D, Zhang Y, Esling C, Hou L, Li X, Zhao X and Zuo L 2020 *Appl. Phys. Lett.* **116** 023902
[49] Wójcik A, Maziarz W, Szczerba M, Kowalczyk M, Cesari E and Dutkiewicz J 2018 *Intermetallics* **100** 88
[50] Zeng Q, Shen J, Zhang H, Chen J, Ding B, Xi X, Liu E, Wang W and Wu G 2019 *J. Phys.: Condens. Matter* **31** 425401
[51] Caron L, Ou Z Q, Nguyen T T, Cam Thanh D T, Tegus O and Brück E 2009 *J. Magn. Magn. Mater.* **321** 3559
[52] Pecharsky V K and Jr. K A G 1997 *Phys. Rev. Lett.* **78** 4494
[53] Hu F, Shen B, Sun J, Cheng Z, Rao G and Zhang X 2001 *Appl. Phys. Lett.* **78** 3675
[54] Liu S, Xuan H, Cao T, Wang L, Xie Z, Liang X, Li H, Feng L, Chen F and Han P 2019 *Phys. Stat. Sol. (a)* **216** 1900563
[55] Li Y, Wei Z Y, Zhang H G, Liu E K, Luo H Z, Liu G D, Xi X K, Wang S G, Wang W H, Yue M, Wu G H and Zhang X X 2016 *APL Mater.* **4** 071101
[56] Kaya M, Yildirim S, Yüzüak E, Dincer I, Ellialtioglu R and Elerman Y 2014 *J. Magn. Magn. Mater.* **368** 191
[57] Zhang Y, Zeng H, Yu G, Liu K, Ma S, Yang K, Zhao X, Yuan G, Luo X, Chen C and Zhong Z 2020 *Intermetallics* **125** 106882
[58] Liu K, Ma S, Ma C, Han X, Yu K, Yang S, Zhang Z, Song Y, Luo X, Chen C, Rehman S U and Zhong Z 2019 *J. Alloys Compd.* **790** 78
[59] Liu Y, Xiao A, Yang T, Xu Z, Zhou X and Ma T 2022 *Scripta Mater.* **207** 114303